International Journal of Solids and Structures 47 (2010) 3389–3396

Contents lists available at ScienceDirect

International Journal of Solids and Structures

journal homepage: www.elsevier.com/locate/ijsolstr

Elasticity with energy limiters for modeling dynamic failure propagation

P. Trapper, K.Y. Volokh *

Faculty of Civil and Environmental Engineering, Technion – Israel Institute of Technology, Haifa 32000, Israel

ARTICLE INFO

Article history:
Received 17 January 2010
Received in revised form 17 August 2010
Available online 21 August 2010

Keywords:
Elasticity
Energy limiters
Dynamics
Failure
Softening
Penetration

ABSTRACT

Separation of two particles is characterized by a magnitude of the bond energy, which limits the accumulated energy of the particle interaction. In the case of a solid composed of many particles a magnitude of the average bond energy – the failure energy – exists, which limits the energy that can be accumulated in an infinitesimal material volume under strain. The energy limiter controls material softening, which indicates failure. Thus, by limiting the stored energy density it is possible to include a description of material failure in the constitutive model. When the failure energy, i.e. the energy limiter, is introduced in the constitutive model it can be calibrated in macroscopic experiments. Traditional elasticity models do not have energy limiters and they allow for the unlimited energy accumulation under the strain increase, which is physically meaningless because no material can sustain large enough strains without failure. We use elasticity with energy limiters for modeling dynamic failure propagation in brittle solids. Two models of isotropic Hookean solids with energy limiters are introduced and examined in simulations of the penetration of a projectile into a brittle plate in the present work. The first model uses the energy limiter with the overall energy term while the second model has separate energy limiters for the volumetric and deviatoric components. The results of the penetration simulation obtained by using both models are similar qualitatively. It is remarkable that the penetration depth is mesh-independent for fine meshes even without the special regularization procedures. This is the first work where the methods of elasticity with energy limiters are used in dynamic analysis of brittle failure.

1. Introduction

Continuum mechanics approaches for modeling material failure can be divided in two groups: surface and bulk models. The surface models, pioneered by Barenblatt (1959), appear by name of Cohesive Zone Models (CZM) in the modern literature. They present material surfaces – cohesive zones – where displacement discontinuities occur. The discontinuities are enhanced with constitutive laws relating normal and tangential displacement jumps with the corresponding tractions. There are a plenty of proposals of constitutive equations for the cohesive zones: Dugdale (1960), Rice and Wang (1989), Tvergaard and Hutchinson (1992), Xu and Needleman (1994) and Camacho and Ortiz (1996), for example. All CZM are constructed qualitatively as follows: tractions increase, reach a maximum, and then approach zero with the increasing separation. Such a scenario is in harmony with our intuitive understanding of the rupture process. Since the work by Needleman (1987) CZM are used increasingly in finite element simulations of crack tip plasticity and creep; crazing in polymers; adhesively bonded joints; interface cracks in bimaterials; delamination in composites and multilayers; fast crack propagation in polymers and etc. Cohesive zones can be inside finite elements or along their boundaries (Xu and Needleman, 1994; Moes et al., 1999; De Borst, 2001). Crack nucleation, propagation, branching, kinking, and arrest are a natural outcome of the computations where the discontinuity surfaces are spread over the bulk material. The latter is in contrast to the traditional approach of fracture mechanics where stress analysis is separated from a description of the actual process of material failure.

The models of bulk failure, pioneered by Kachanov (1958, 1986), Rabotnov (1963), appear by name of Continuum Damage Mechanics (CDM) in the modern literature. Originally, CDM aimed at analysis of the gradual failure accumulation and propagation in *creep* and *fatigue* and it appeared almost simultaneously with the cohesive zone approach. The need to describe the failure *accumulation*, i.e. evolution of the material microstructure, explains why CDM is very similar to plasticity theories including (a) the internal damage variable (inelastic strain), (b) the critical threshold condition (yield surface), and (c) the damage evolution equation (flow rule). The subsequent development of the formalism of CDM (summarized in: Krajcinovic, 1996; Skrzypek and Ganczarski, 1999; Lemaitre and Desmorat, 2005) left its physical origin well behind the mathematical and computational techniques and, eventually, led to the use of CDM for the description of *any* bulk failure – see a discussion by Kachanov (1994). Theoretically, the approach

* Corresponding author. Tel.: +972 4 8292426; fax: +972 4 8295697.
E-mail address: cvolokh@technion.ac.il (K.Y. Volokh).

0020-7683/$ - see front matter © 2010 Elsevier Ltd. All rights reserved.
doi:10.1016/j.ijsolstr.2010.08.016

of CDM is very flexible and it allows reflecting physical processes triggering macroscopic damage at small length scales. Practically, the experimental calibration of CDM is not trivial because it is difficult to measure the damage parameter directly. The experimental calibration should be implicit and include both the damage evolution equation and criticality condition.

A physically-motivated alternative to damage mechanics in the cases of failure related with the bond rupture has been considered recently by Gao and Klein (1998), Klein and Gao (1998) who showed how to mix the atomic/molecular and continuum descriptions in order to simulate material failure. They applied the so-called Cauchy–Born rule linking micro- and macro- scales to empirical potentials, which include a possibility of the full atomic separation. The continuum-atomistic link led to the formulation of the macroscopic strain energy potentials allowing for the stress/strain softening and strain localization. The continuum-atomistic method is effective at small length scales where purely atomistic analysis becomes computationally intensive. Unfortunately, a direct use of the continuum-atomistic method in macroscopic failure problems is not very feasible because its computer implementation includes a numerically involved procedure of the averaging of the interatomic potentials over a representative volume. In order to bypass the computational intensity of the continuum-atomistic method while preserving its sound physical basis the *softening hyperelasticity* approach was developed by Volokh (2004), Volokh (2007), Volokh (2008b). The basic idea of softening hyperelasticity is to formulate an expression of the stored macroscopic energy, which would include the energy limiter(s) – the average bond energy. Such a limiter automatically induces strain softening, that is a material failure description, in the constitutive law.

To motivate the introduction of energy limiters we briefly describe the continuum-atomistic link. A more detailed exposition of the issue can be found in Volokh (2008b), for example.

Interaction of two particles (atoms, molecules, etc.) can be described as follows:

$$\psi(F) = \varphi(F) - \varphi_0, \quad \varphi_0 = \min_L \varphi(F = 1). \tag{1.1}$$

Here ψ is the particle interaction potential; F is the one-dimensional deformation gradient which maps the distance between particles from the reference, L, to the current, l, state: $l = FL$. To be specific we choose the Lennard–Jones potential, for example, $\varphi = 4\varepsilon[(\sigma/l)^{12} - (\sigma/l)^6]$, where ε and σ are the bond energy and length constants accordingly. By direct computation we can find the energy limiter or the failure energy, Φ. Indeed, increasing deformation we cannot increase the energy unlimitedly

$$\psi(F \to \infty) = -\varphi_0 = \Phi = \text{constant}. \tag{1.2}$$

Analogously to the case of the pair interaction it is possible to consider particle assemblies. Applying the assumption of applicability of continuum mechanics to the description of such assemblies, i.e. using the Cauchy–Born rule, it is possible to derive the following stored energy function analogously to (1.1)

$$\psi(\mathbf{C}) = \langle\varphi(\mathbf{C})\rangle - \langle\varphi\rangle_0, \quad \langle\varphi\rangle_0 = \min_L \langle\varphi(\mathbf{C} = \mathbf{1})\rangle. \tag{1.3}$$

Here $\mathbf{C} = \mathbf{F}^T\mathbf{F}$ is the right Cauchy–Green deformation tensor where $\mathbf{F} = \partial\mathbf{y}/\partial\mathbf{x}$ is the deformation gradient of a generic material macro-particle of body Ω occupying position $\mathbf{x}$ at the reference state and position $\mathbf{y}(\mathbf{x})$ at the current state of deformation. The average in (1.3) is defined as $\langle\varphi(\mathbf{C})\rangle = V_0^{-1}\int_{V_0^*} 4\varepsilon[(\sigma/L\|\mathbf{C}\|)^{12} - (\sigma/L\|\mathbf{C}\|)^6]D_V dV$ in the case of the Lennard–Jones potential, where the tensorial norm designates stretch in the bond direction; D_V is the volumetric bond density function; and V_0^* is the integration volume defined by the range of influence of φ; and V_0 is the reference representative volume.

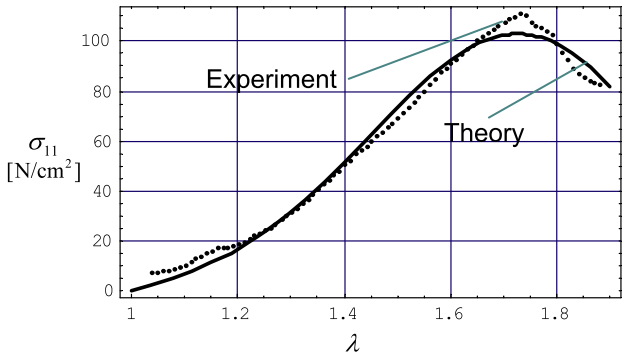

Fig. 1. Theory versus experiment for uniaxial tension of AAA material. σ_{11} and λ are the axial Cauchy stress and stretch accordingly (Volokh and Vorp, 2008).

Analogously to (1.2), we can find the energy limiter, Φ, increasing the deformation unlimitedly

$$\Phi = \psi(\|\mathbf{C}\| \to \infty) = -\langle\varphi\rangle_0 = \text{constant}. \tag{1.4}$$

Thus, *the average bond energy sets a limit for the energy accumulation*. This conclusion generally does not depend on the choice of the particle potential and it is valid for any interaction that includes a possible particle separation.

Contrary to the conclusion above traditional hyperelastic models of materials do not include the energy limiter. The stored energy of hyperelastic materials is defined as:

$$\psi = W. \tag{1.5}$$

Here W is used for the strain energy of the *intact* material, which can be characterized as follows:

$$\|\mathbf{C}\| \to \infty \Rightarrow \psi = W \to \infty, \tag{1.6}$$

where $\|\ldots\|$ is a tensorial norm.[1]

In other words, the increasing strain increases the accumulated energy unlimitedly. Evidently, the consideration of only intact materials is restrictive and unphysical. The energy increase of a real material should be limited as it was shown above,

$$\|\mathbf{C}\| \to \infty \Rightarrow \psi \to \Phi = \text{constant}, \tag{1.7}$$

where the average bond energy, Φ = constant, can be called the *material failure energy*.

Eq. (1.7) presents the fundamental idea of introducing a limiter of the stored energy in the elasticity theory. Such a limiter induces material softening, indicating material failure, automatically. *The choice of the limited stored energy expression should generally be material/problem-specific.*

An example of the experimental calibration of energy limiters can be found in Volokh and Vorp (2008) for the case of the material of abdominal aortic aneurysm (AAA). AAA is rubberlike and its strain energy can be written as follows: $\psi = \Phi - \Phi\exp(-\alpha_1(\mathrm{tr}\mathbf{C} - 3)/\Phi - \alpha_2(\mathrm{tr}\mathbf{C} - 3)^2/\Phi)$, where α_1 and α_2 are the elasticity constants of the material; and Φ is the energy limiter (failure energy). The uniaxial tension test results are shown in Fig. 1, where the model was fitted with the following constants: $\alpha_1 = 10.3$ N/cm^2; $\alpha_2 = 18.0$ N/cm^2; $\Phi = 40.2$ N/cm^2. It is worth emphasizing that energy limiters set failure energy per unit *volume* contrary to the traditional approach which sets failure energy per unit *area*.

The softening hyperelasticity approach is computationally simple yet physically appealing. The approach proved itself in a number of problems varying from failure of brittle materials to rubbers and soft biological tissues[2]: Volokh (2004), Volokh (2007), Volokh

[1] We do not specify the tensorial norm intentionally because various norms can be used.

[2] More sophisticated models to control softening are presented in Trapper and Volokh (2010), for example.

(2008a), Volokh (2008b), Trapper and Volokh (2008), Trapper and Volokh (2009), Volokh and Trapper (2008), Volokh and Vorp (2008). Besides, Gei et al. (2004), Gearing and Anand (2004) used variants of hyperelasticity with softening in the context of ductile and ductile–brittle failure accordingly. One should be careful, however, with treating ductile behavior by using energy limiters because material failure during plastic deformation is essentially due to microstructural changes rather than the bond rupture. The latter means that the approach of energy limiters may not be applicable in the case of inelasticity on physical grounds.

All mentioned works use elasticity with energy limiters for the prediction of the global material/structural instability. The present work aims at extending the approach to the problems of the dynamic failure propagation. The outline of the paper is as follows. In Section 2 we introduce two different models of the Hookean solid with energy limiters and discuss their features by considering deformations under hydrostatic tension/compression and simple shear In Section 3 we present the results of 3D simulations of the high-velocity penetration of an elastic–plastic projectile into a brittle plate described by the introduced models of elasticity with energy limiters. We compare the results for the different models and monitor the influence of mesh size on the depth of the projectile penetration. The general discussion of the proposed approaches and simulation results is present in Section 4.

2. Hookean elasticity with energy limiters

The Hookean elasticity defined below is a limit case (after linearization) for any theory embedding the energy limiters

$$W=\frac{\lambda}{2}(\mathrm{tr}\boldsymbol{\varepsilon})^2+\mu\boldsymbol{\varepsilon}:\boldsymbol{\varepsilon}=\frac{K}{2}(\mathrm{tr}\boldsymbol{\varepsilon})^2+\mu\mathbf{e}:\mathbf{e}, \tag{2.1}$$

$$\boldsymbol{\sigma}=\frac{\partial W}{\partial\boldsymbol{\varepsilon}}=\lambda(\mathrm{tr}\boldsymbol{\varepsilon})\mathbf{1}+2\mu\boldsymbol{\varepsilon}=K(\mathrm{tr}\boldsymbol{\varepsilon})\mathbf{1}+2\mu\mathbf{e}, \tag{2.2}$$

$$\mathbf{e}=\boldsymbol{\varepsilon}-\frac{\mathrm{tr}\boldsymbol{\varepsilon}}{3}\mathbf{1}, \tag{2.3}$$

$$2\boldsymbol{\varepsilon}=\frac{\partial\mathbf{u}}{\partial\mathbf{x}}+\left(\frac{\partial\mathbf{u}}{\partial\mathbf{x}}\right)^T, \tag{2.4}$$

where W is the strain energy; $\boldsymbol{\sigma}$ is the Cauchy stress tensor; $\mathbf{1}$ is the identity tensor; $\mathbf{e}$ is the deviator of the small strain tensor $\boldsymbol{\varepsilon}$; $\mathbf{u}=\mathbf{y}(\mathbf{x})-\mathbf{x}$ is the displacement vector; $K=\lambda+\frac{2}{3}\mu$ is the bulk modulus; $\lambda=\frac{Ev}{(1+v)(1-2v)}$ and $\mu=\frac{E}{2(1+v)}$ are the Lame moduli; E is the Young modulus; and v is the Poisson ratio.

In what follows we modify (2.1) enforcing various descriptions of material failure.

2.1. The 1st model with energy limiters

The first model with the energy limiter, Φ, takes the following form

$$\psi=\Phi-\Phi\left(1+\sqrt{\frac{K}{\Phi}}\mathrm{tr}\boldsymbol{\varepsilon}\right)\exp\left(-\sqrt{\frac{K}{\Phi}}\mathrm{tr}\boldsymbol{\varepsilon}-\frac{\mu}{\Phi}\mathbf{e}:\mathbf{e}\right), \tag{2.5}$$

$$\boldsymbol{\sigma}=\frac{\partial\psi}{\partial\boldsymbol{\varepsilon}}=\tilde{K}(\mathrm{tr}\boldsymbol{\varepsilon})\mathbf{1}+2\tilde{\mu}\mathbf{e}, \tag{2.6}$$

where

$$\tilde{K}=K\exp\left(-\sqrt{\frac{K}{\Phi}}\mathrm{tr}\boldsymbol{\varepsilon}-\frac{\mu}{\Phi}\mathbf{e}:\mathbf{e}\right), \tag{2.7}$$

$$\tilde{\mu}=\mu\left(1+\sqrt{\frac{K}{\Phi}}\mathrm{tr}\boldsymbol{\varepsilon}\right)\exp\left(-\sqrt{\frac{K}{\Phi}}\mathrm{tr}\boldsymbol{\varepsilon}-\frac{\mu}{\Phi}\mathbf{e}:\mathbf{e}\right). \tag{2.8}$$

When linearized the model reduces to the Hooke law, (2.1) and (2.2): $\tilde{K}=K$ and $\tilde{\mu}=\mu$.

Targeting simulations of the dynamic failure processes it is important to complete the model with criteria for dropping failed finite elements. We choose specifically

$$\psi\geqslant\Phi\quad\text{and}\quad\|\boldsymbol{\sigma}\|=\sqrt{\boldsymbol{\sigma}:\boldsymbol{\sigma}}=0. \tag{2.9}$$

This criterion takes into account a possibility of the unbounded energy accumulation under hydrostatic compression. In the latter case the stored energy can exceed the limiting value without the decline in stresses.

We consider two simple homogeneous deformations to get better insight in the presented material model. We start with the hydrostatic tension/compression. In this case we have $\varepsilon_{11}=\varepsilon_{22}=\varepsilon_{33}$ and $\sigma_{11}=\sigma_{22}=\sigma_{33}$ and the constitutive law reduces to

$$\sigma_{11}=3K\varepsilon_{11}\exp\left(-\sqrt{\frac{K}{\Phi}}3\varepsilon_{11}\right). \tag{2.10}$$

Fig. 2 presents (2.10) graphically for a sample brittle material: $E=315{,}000$ MPa; $v=0.24$; $\Phi=0.65$ MPa.

It is easily observed that failure starts at the limit point in tension and it is completed at the starred point where the criteria for dropping failed finite elements, (2.9), are obeyed. There is no material failure in pure hydrostatic compression.

Now we consider simple shear. In this case we have only $\varepsilon_{12}=\varepsilon_{21}$ and $\sigma_{12}=\sigma_{21}$ and the constitutive law reduces to

$$\sigma_{12}=2\mu\varepsilon_{12}\exp\left(-2\frac{\mu}{\Phi}\varepsilon_{12}^2\right). \tag{2.11}$$

Fig. 3 presents (2.10) graphically for a sample material: $E=315{,}000$ MPa; $v=0.24$; $\Phi=0.65$ MPa.

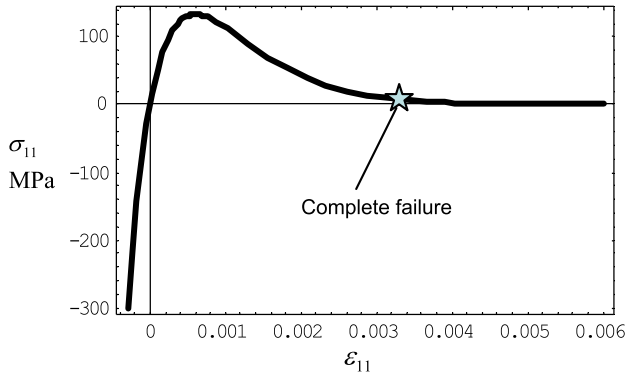

Fig. 2. Stress–strain curve in hydrostatic tension/compression: the complete failure criteria (2.9) are met at the starred point.

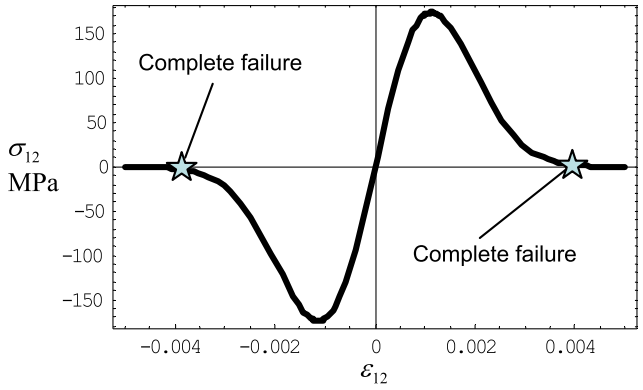

Fig. 3. Stress–strain curve in simple shear: the complete failure criteria (2.9) are met at the starred points.

Failure starts at the limit points and it is completed at the starred points where the criteria for dropping failed finite elements, (2.9), are obeyed.

Remark 1. In computations we set value $Tol = 10^{-5}$ for zero tolerance in $(2.9)_2$: $\|\sigma\| \leqslant Tol$. Dropping the failed elements is necessary in order to prevent from the material healing when a returning wave of deformation can restore the failed elements. The element 'killing' or removing procedure is an integral part of the available finite element software dealing with the failure simulations. Usually, the elements are removed forcefully when a criterion of the removal is obeyed. In our case, however, contrary to the widespread finite element technologies there is no need to kill the elements – they die on their own – and it is only necessary remove the failed elements.

2.2. The 2nd model with energy limiters

The second model introduces separate failure modes related with volumetric and shape changes with the help of two energy limiters, Φ_1 and Φ_2,

$$\psi = \psi_1 + \psi_2, \tag{2.12}$$

$$\psi_1 = \Phi_1 - \Phi_1\left(1 + \sqrt{\frac{K}{\Phi_1}}\mathrm{tr}\,\boldsymbol{\varepsilon}\right)\exp\left(-\sqrt{\frac{K}{\Phi_1}}\mathrm{tr}\,\boldsymbol{\varepsilon}\right), \tag{2.13}$$

$$\psi_2 = \Phi_2 - \Phi_2\exp\left(-\frac{\mu}{\Phi_2}\mathbf{e}:\mathbf{e}\right), \tag{2.14}$$

$$\boldsymbol{\sigma} = \frac{\partial\psi}{\partial\boldsymbol{\varepsilon}} = \widetilde{K}(\mathrm{tr}\,\boldsymbol{\varepsilon})\mathbf{1} + 2\tilde{\mu}\mathbf{e}, \tag{2.15}$$

where

$$\widetilde{K} = K\exp\left(-\sqrt{\frac{K}{\Phi_1}}\mathrm{tr}\,\boldsymbol{\varepsilon}\right), \tag{2.16}$$

$$\tilde{\mu} = \mu\exp\left(-\frac{\mu}{\Phi_2}\mathbf{e}:\mathbf{e}\right). \tag{2.17}$$

When linearized the model reduces to the Hooke law, (2.1) and (2.2): $\widetilde{K} = K$ and $\tilde{\mu} = \mu$.

We choose the following criteria of the element failure

$$\psi_1 \geqslant \Phi_1 \quad \text{and} \quad |\mathrm{tr}\,\boldsymbol{\sigma}| = 0 \quad \text{or} \quad \psi_2 = \Phi_2. \tag{2.18}$$

The first criterion takes into account the possibility of the unbounded energy accumulation under hydrostatic compression as in the case of the 1st model in the previous subsection. The second criterion is related with the distortional failure.

In the case of the hydrostatic tension/compression we have $\varepsilon_{11} = \varepsilon_{22} = \varepsilon_{33}$ and $\sigma_{11} = \sigma_{22} = \sigma_{33}$ and the constitutive law reduces to

$$\sigma_{11} = 3K\varepsilon_{11}\exp\left(-\sqrt{\frac{K}{\Phi_1}}3\varepsilon_{11}\right). \tag{2.19}$$

Fig. 4 presents (2.19) graphically for a sample brittle material: $E = 315{,}000$ MPa; $\nu = 0.24$; $\Phi_1 = 0.55$ MPa.

Failure starts at the limit point in tension and it is completed at the starred point where the criteria for dropping failed finite elements, (2.18), are obeyed. There is no material failure in pure hydrostatic compression.

In this case of simple shear we have $\varepsilon_{12} = \varepsilon_{21}$ and $\sigma_{12} = \sigma_{21}$ and the constitutive law reduces to

$$\sigma_{12} = 2\mu\varepsilon_{12}\exp\left(-2\frac{\mu}{\Phi_2}\varepsilon_{12}^2\right). \tag{2.20}$$

Fig. 5 presents (2.20) graphically for a sample brittle material: $E = 315{,}000$ MPa; $\nu = 0.24$; $\Phi_2 = 0.45$ MPa.

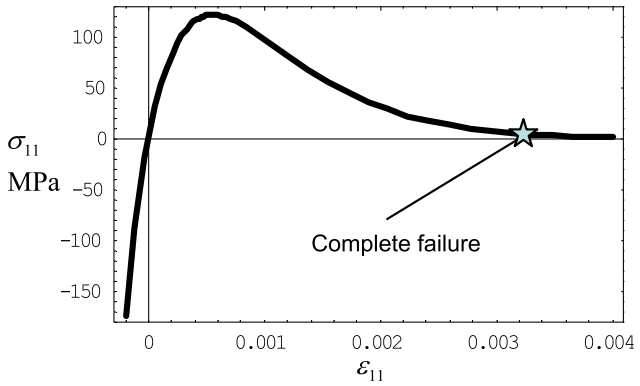

Fig. 4. Stress–strain curve in hydrostatic tension/compression: the complete failure criteria (2.18) are met at the starred point.

Failure starts at the limit points and it is completed at the starred points where the criteria for dropping failed finite elements, (2.18), are obeyed.

3. Dynamic failure simulations

We implement the described analytical models with the help of the user defined subroutine VUMAT within ABAQUS/EXPLICIT (2008) finite element software. It is important to emphasize that during the process of material failure some finite elements can undergo large Rigid Body Motion (RBM) without developing large stretches/strains. RBM can distort the results of analysis if the small deformation formulations of the previous section are adopted. To suppress the influence of RBM in numerical simulations it is possible, for example, to replace the linear strain, $\boldsymbol{\varepsilon}$, with the Green strain

$$\mathbf{E} = \frac{1}{2}(\mathbf{F}^T\mathbf{F} - \mathbf{1}) = \frac{1}{2}(\mathbf{U}^2 - \mathbf{1}). \tag{3.1}$$

Here the polar decomposition of the deformation gradient, $\mathbf{F} = \mathbf{RU}$, is used where the proper orthogonal tensor, $\mathbf{R}$, represents local rotations and the symmetric positive definite tensor, $\mathbf{U}$, represents local stretching. Evidently, the Green strain is not affected by RBM and, moreover it approximately coincides with the linear strain for small deformations.

Substituting the Green strain in the strain energy functions introduced in the previous section we obtain the 2nd Piola–Kirchhoff stress

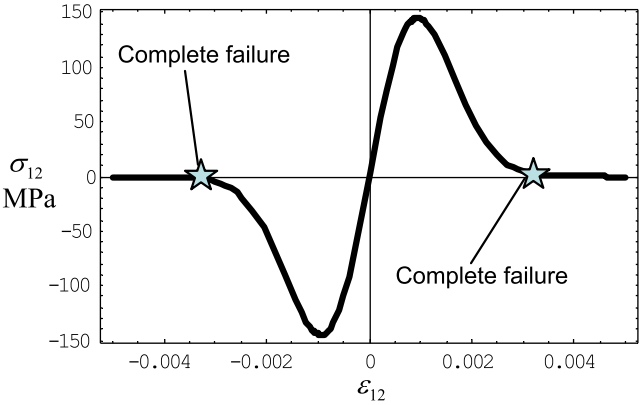

Fig. 5. Stress–strain curve in simple shear: the complete failure criteria (2.18) are met at the starred points.

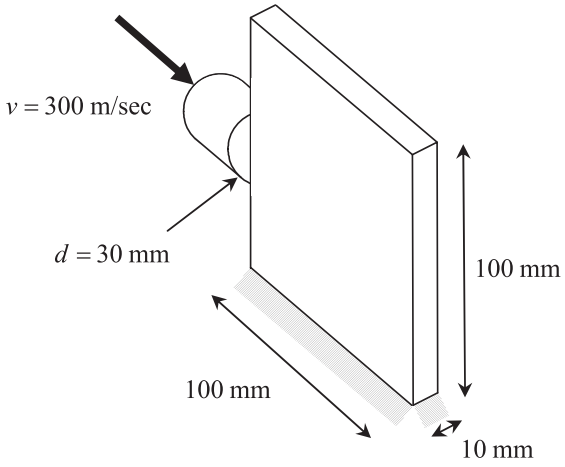

Fig. 6. High-velocity penetration of a projectile into a brittle plate.

$$\mathbf{S} = \frac{\partial \psi(\mathbf{E})}{\partial \mathbf{E}}, \tag{3.2}$$

which is related to the Cauchy stress as follows:

$$\boldsymbol{\sigma} = (\det \mathbf{F})^{-1} \mathbf{F}\mathbf{S}\mathbf{F}^{T}. \tag{3.3}$$

It is important that in the considered cases of brittle materials the stretching is small, which implies

$$\boldsymbol{\sigma} \cong \mathbf{R}\mathbf{S}\mathbf{R}^{T}, \tag{3.4}$$

or

$$\mathbf{S} \cong \mathbf{R}^{T}\boldsymbol{\sigma}\mathbf{R}. \tag{3.5}$$

The latter equation means that the 2nd Piola–Kirchhoff stress is equal to the Cauchy stress rotated to the reference configuration. Thus, **S** has a clear and convenient physical meaning.[3] Obviously, the material failure indicators are invariant with respect to the choice of $\boldsymbol{\sigma}$ or **S** in computations.

We simulate 3D impact and penetration of a cylindrical projectile on the edge of a plate fixed at its bottom – Fig. 6.

The projectile is elastic–plastic with mass density, $\rho = 7.85$ g/cm^3; elasticity modulus, $E = 207{,}000$ MPa; Poisson ratio, $\nu = 0.3$; and the stress–strain curve defined in Fig. 7.

The brittle plate has mass density, $\rho = 3.67$ g/cm^3; elasticity modulus, $E = 315{,}000$ MPa; Poisson ratio, $\nu = 0.24$; and its constitutive models have been defined in the previous section. Since the plate is thin the failed material is not stored and there is no need to consider its hydrostatic resistance.

We present four series – Figs. 8–11 – of dynamic simulations of impact at the velocity of 300 m/s by using different meshes.

The first series of simulations presented in Fig. 8 is based on the first material model with energy limiters with failure energy, $\Phi = 0.65$ MPa. We use three variants of the 3D finite element mesh: the coarse mesh of $21{,}600 = 60 \times 60 \times 6$ brick elements; the intermediate mesh of $51{,}200 = 80 \times 80 \times 8$ is 80 brick elements; and the fine mesh of $100{,}000 = 100 \times 100 \times 10$ brick elements. The plate is cut into two pieces. During penetration a cavity is created in front of the projectile, which propagates and leads to the total fracture – Fig. 8a. The dissipated energy is presented in the dimensionless form in Fig. 8b where it is shown how the relative volume of the eroded elements evolves in time. In order to calculate the absolute value of the dissipated energy it is necessary to multiply the absolute volume of the eroded elements by the constant of the failure energy, $\Phi = 0.65$ MPa.

[3] Similar situation takes place in the case of stiff yet flexible thin-walled structures.

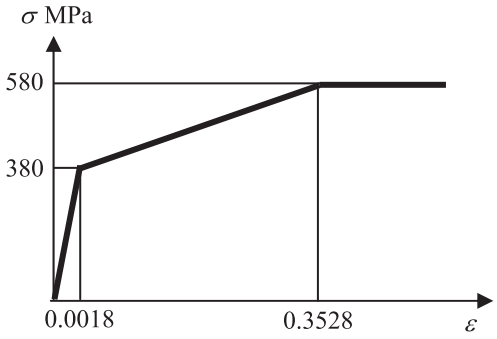

Fig. 7. Constitutive description of the elastic–plastic projectile.

Similar results are observed in the second series of simulations presented in Fig. 9, which is based on the second material model with energy limiters and failure energies, $\Phi_1 = 0.55$ MPa and $\Phi_2 = 0.45$ MPa. 3D meshes of $21{,}600 = 60 \times 60 \times 6$; $51{,}200 = 80 \times 80 \times 8$; and $100{,}000 = 100 \times 100 \times 10$ brick elements have been used. All element failures occurred in distortion when elements reached the critical failure energy $\Phi_2 = 0.45$ MPa. In order to calculate the absolute value of the dissipated energy it is necessary to multiply the absolute volume of the eroded elements shown in Fig. 9b by $\Phi_2 = 0.45$ MPa.

Though the similarity in the projectile propagation has been observed for various meshes it is interesting to analyse the depth of the penetration when the projectile stops without cutting the plate completely. For this purposes we increased the magnitude of failure energies. The third series of simulations presented in Fig. 10 is based on the first material model with failure energy: $\Phi = 1.3$ MPa. We use three 3D finite element meshes of $100{,}000 = 100 \times 100 \times 10$; $274{,}400 = 140 \times 140 \times 14$; and $583{,}200 = 180 \times 180 \times 18$ brick elements. The projectile penetrates approximately to the middle of the plate without cutting it. There is a slight effect of the mesh size: the coarse mesh is a bit stiffer.

Similar results on the arrested penetration are observed in the fourth series of simulations presented in Fig. 11, which is based on the second material model with failure energies, $\Phi_1 = 1.1$ MPa and $\Phi_2 = 0.9$ MPa. Again, we use three 3D finite element meshes of $100{,}000 = 100 \times 100 \times 10$; $274{,}400 = 140 \times 140 \times 14$; and $583{,}200 = 180 \times 180 \times 18$ brick elements and observe that the coarse mesh leads to a stiffer response while the intermediate and fine meshes provide similar results. Again, all element failures occurred in distortion when elements reached the critical failure energy $\Phi_2 = 0.9$ MPa. In order to calculate the absolute value of the dissipated energy it is necessary to multiply the absolute volume of the eroded elements shown in Fig. 11b by $\Phi_2 = 0.9$ MPa.

4. Discussion

The Hookean model of brittle solids allows material to accumulate strain energy unlimitedly. The latter is unphysical and the possibility of material failure should be included in the theoretical description. A way to describe failure is to introduce energy limiters in the expression of the strain energy. This idea is essentially an extension of the description of two particle separation to large amounts of particles – continuum. The methods of elasticity with energy limiters are dramatically simpler than the existing methods of Continuum Damage Mechanics, for example, that are traditionally used for modeling bulk failure. We strongly emphasize, however, that the elasticity with energy limiters is not a universal substitute for Continuum Damage Mechanics. Materials exhibiting essential structural changes during deformation, e.g. plasticity, creep, fatigue, are beyond the scope of the methods

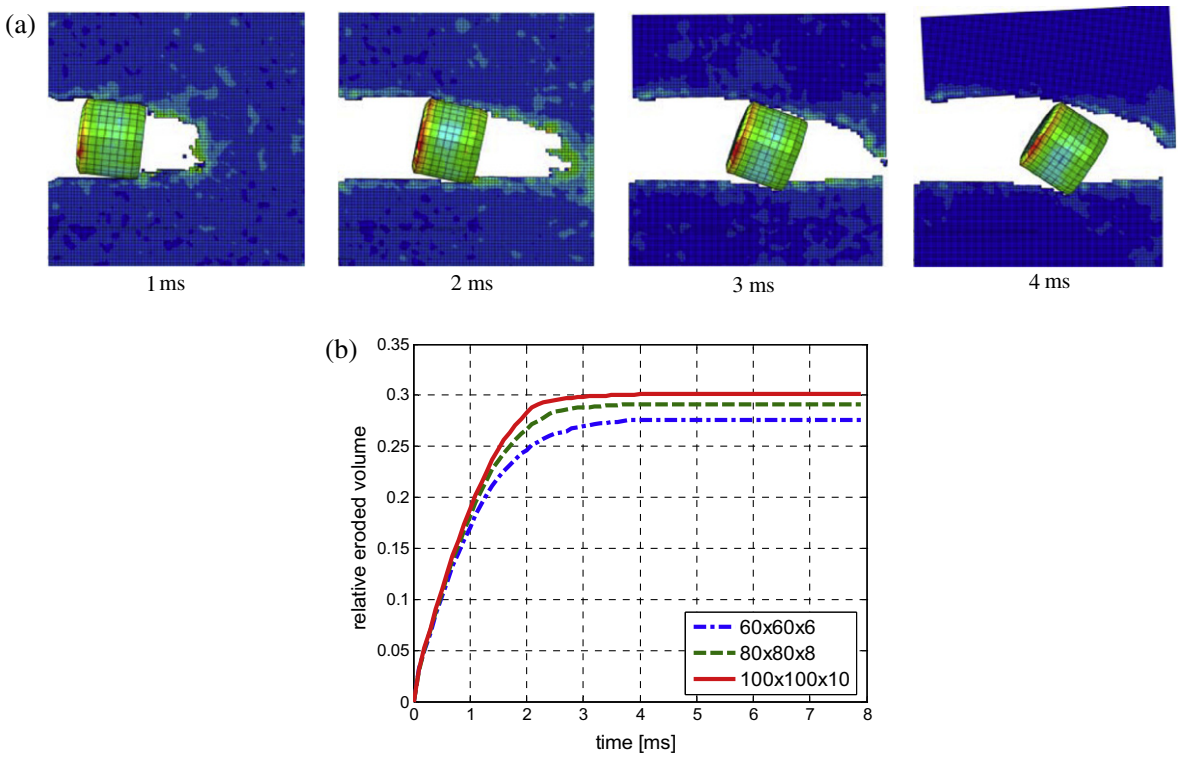

Fig. 8. Projectile penetration in the case of the first material model with $\Phi = 0.65$ MPa: (a) accumulated failure at 1, 2, 3, and 4 ms, (b) relative eroded volume (dissipated energy) for various finite element meshes.

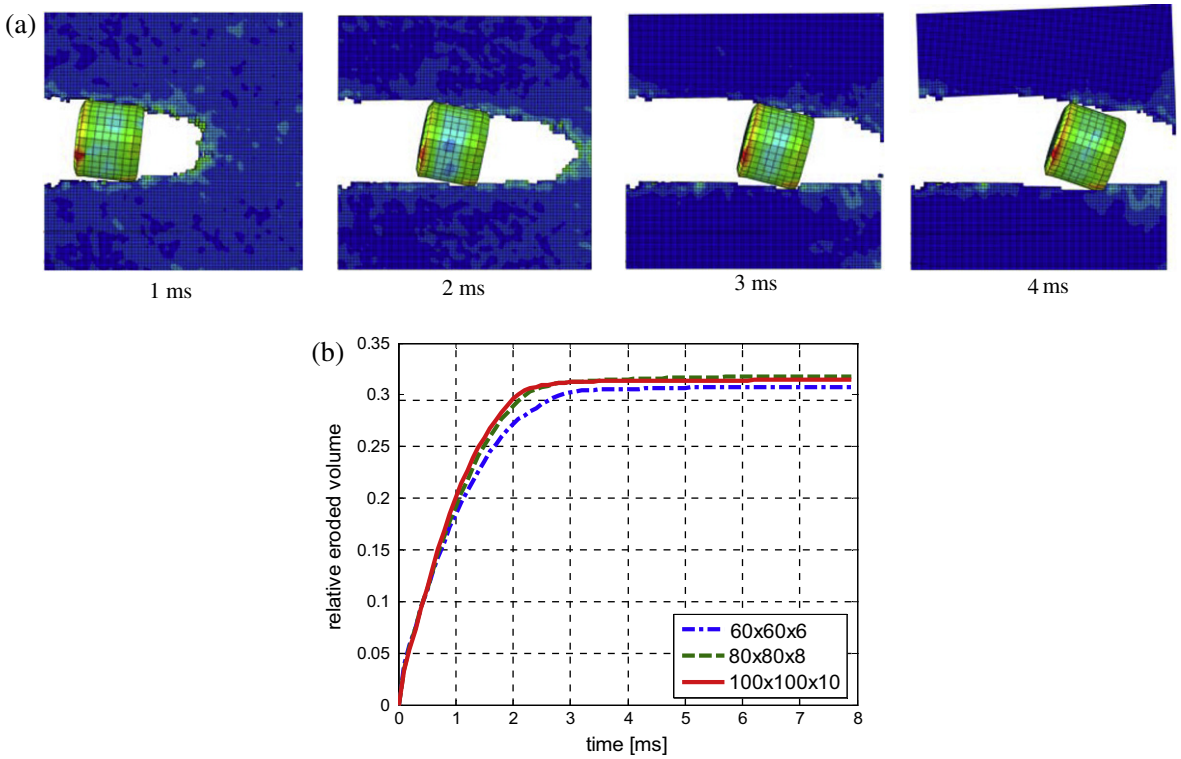

Fig. 9. Projectile penetration in the case of the second material model with $\Phi_1 = 0.55$ MPa and $\Phi_2 = 0.45$ MPa: (a) accumulated failure at 1, 2, 3, and 4 ms, (b) relative eroded volume (dissipated energy) for various finite element meshes.

of energy limiters, which do not describe the structural changes in materials except for the complete failure because of the bond rupture.

Elasticity with energy limiters is an example of material models with softening. Generally, material models with softening have been extensively discussed in the literature. It is clear from the

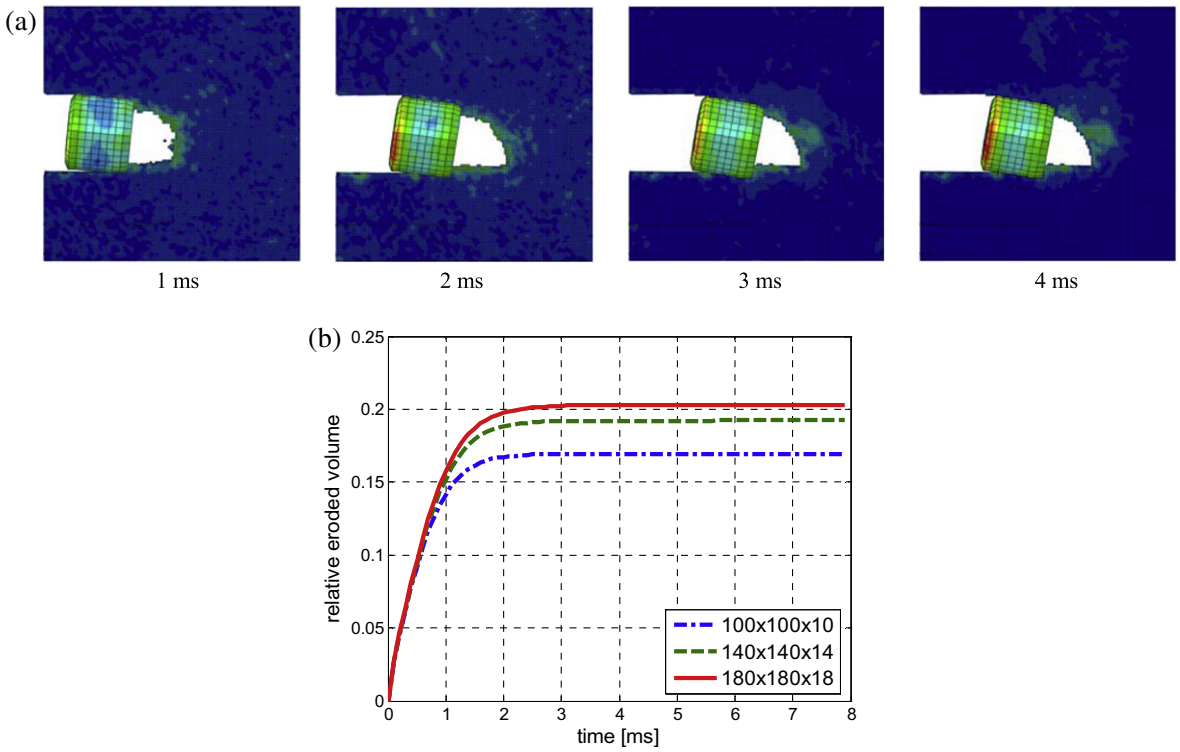

Fig. 10. Projectile penetration in the case of the first material model with $\Phi = 1.3$ MPa: (a) accumulated failure at 1, 2, 3, and 4 ms, (b) relative eroded volume (dissipated energy) for various finite element meshes.

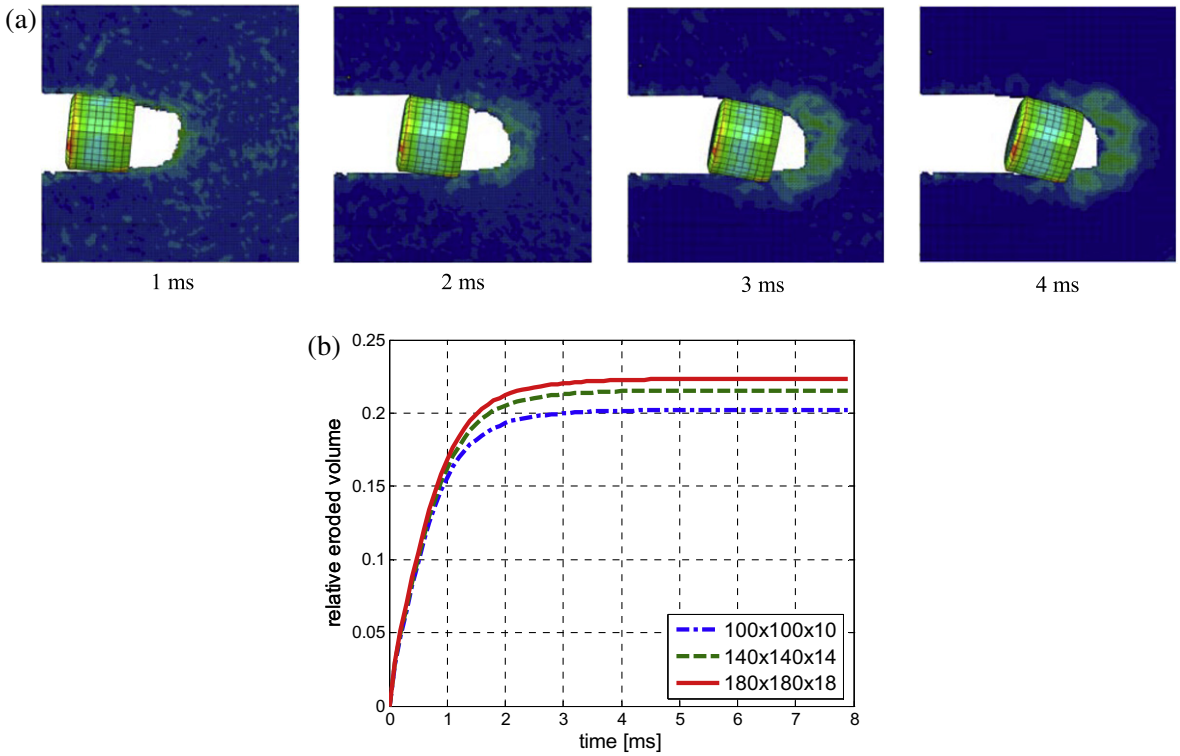

Fig. 11. Projectile penetration in the case of the second material model with $\Phi_1 = 1.1$ MPa and $\Phi_2 = 0.9$ MPa: (a) accumulated failure at 1, 2, 3, and 4 ms, (b) relative eroded volume (dissipated energy) for various finite element meshes.

discussions that such models fail to predict, for example, the width of the shear band without introducing a characteristic material length. The reason is that the physical processes triggering the band formation take place at the length scales where the classical length-independent continuum mechanics may not be applicable. Extrapolating from the shear band example, the whole approach

of the constitutive equations with softening within the framework of the classical/local continuum mechanics was questioned. It was argued that the models with softening exhibit the 'pathological' mesh-sensitivity in the finite element analysis. That meant specifically that the results of computations would not converge to a limit under the mesh refinement. For example, the width of the failure zone localized within a strip of one element width would decrease with the mesh refinement. The latter observation can be interpreted as follows: the finite element meshes 'search' for the minimum failure size and cannot find it. Such mesh-sensitivity indicates that deformation tends to localize in material volumes smaller than the representative ones[4] or, in other words, the pathological mesh-sensitivity is an indicator of the failure the classical/local continuum mechanics. The results of our computations show that failure may not tend to localize sharply in material volumes smaller than the representative material volumes of continuum mechanics and, consequently, there is no pathological mesh-sensitivity. No sharp localization – no pathology. Even in the absence of sharp localizations or in the cases where such localizations are directly enforced in analysis high strain gradients and the bifurcation multiplicity are two main sources of mesh-sensitivity. Evidently the necessity to treat high strain gradients by refining the mesh is not specific of the material models with softening – this is the central issue of the finite element analysis as a whole. The bifurcation multiplicity, which means that the solution of the governing equations splits into multiple branches at a critical bifurcation point, is more typical of the models with softening. It is worth noting that both bulk and surface (cohesive zone) models can suffer from the bifurcation multiplicity. The latter may trigger some uncertainty, i.e. mesh dependency, of numerical simulations. It seems reasonable to assume that the numerical uncertainty reflects the real physical uncertainty of the problem of material failure. One can regularize mathematics not physics.

Finally, we emphasize again that the developed approach aims at modeling the massive bulk failure that cannot be tackled by the cohesive zone or embedded discontinuity approach, which prescribes the appearance of cracks in advance. It is probably possible to extend the considered approach to modeling sharp localizations – cracks. The main complexity here is that the elasticity with energy limiters (as well as the classical continuum damage mechanics) does not possess a characteristic length. The latter is the reason why results of the finite element simulations will depend on the size, h, of the element when failure tends to localize in narrow zones – cracks. To make the calculations objective it is necessary to derive the physically reasonable value of the element size. Let us assume that the volumetric failure energy is Φ and, consequently, the energy dissipated by one spatial element is $\sim \Phi h^3$. If failure localizes into a surface with the *surface failure energy* G then the dissipated element energy is $\sim Gh^2$. Equalizing both element energies, we get the element size: $h \sim G/\Phi$. Of course, the derivation of G requires tests where the failure localization is controlled by the preexisting notches, for example. Alternatively, other regularization procedures can be considered. For example, the regularization can be based on the generalized continuum formulation embedding the characteristic length – higher-order, gradient, or non-local theories (de Borst and van der Giessen, 1998); or the Hillerborg et al. (1976) approach where a characteristic length is introduced directly in the finite element model; or, possibly, by introducing the rate dependence in the constitutive or balance equations (Needleman, 1988; Zhang et al., 2002).

[4] We do not specify the size of the representative volume though that is possible for every specific material.

Acknowledgement

This work was reported at the IUTAM 2009 Symposium on Dynamic Fracture and Fragmentation at Austin, Texas, and it benefited from the fruitful discussions with the participants.

This research was supported by the Israeli Ministry of Construction and Housing.

References

ABAQUS, Version 6.8, 2008. H.K.S Inc., Pawtucket, RI.
Barenblatt, G.I., 1959. The formation of equilibrium cracks during brittle fracture. General ideas and hypotheses. Axially-symmetric cracks. J. Appl. Math. Mech. 23, 622–636.
Camacho, G.T., Ortiz, M., 1996. Computational modeling of impact damage in brittle materials. Int. J. Solids Struct. 33, 2899–2938.
De Borst, R., 2001. Some recent issues in computational failure mechanics. Int. J. Numer. Meth. Eng. 52, 63–95.
de Borst, R., van der Giessen, E., 1998. Material Instabilities in Solids. Wiley, Chichister.
Dugdale, D.S., 1960. Yielding of steel sheets containing slits. J. Mech. Phys. Solids 8, 100–104.
Gao, H., Klein, P., 1998. Numerical simulation of crack growth in an isotropic solid with randomized internal cohesive bonds. J. Mech. Phys. Solids 46, 187–218.
Gearing, B.P., Anand, L., 2004. Notch-sensitive fracture of polycarbonate. Int. J. Solids Struct. 41, 827–845.
Gei, M., Bigoni, D., Guicciardi, S., 2004. Failure of silicon nitride under uniaxial compression at high temperature. Mech. Mat. 36, 335–345.
Hillerborg, A., Modeer, M., Peterson, P.E., 1976. Analysis of crack growth in concrete by means of fracture mechanics and finite elements. Cement Concrete Res. 6, 773–782.
Kachanov, L.M., 1958. Time of the rupture process under creep conditions. Izvestiya Akademii Nauk SSSR, Otdelenie Teckhnicheskikh Nauk 8, 26–31. in Russian.
Kachanov, L.M., 1986. Introduction to continuum damage mechanics. Martinus Nijhoff, Dotrecht, Netherlands.
Kachanov, M., 1994. On the concept of damage in creep and in the brittle–elastic range. Int. J. Damage Mech. 3, 329–337.
Klein, P., Gao, H., 1998. Crack nucleation and growth as strain localization in a virtual-bond continuum. Eng. Fract. Mech. 61, 21–48.
Krajcinovic, D., 1996. Damage mechanics. Series in Applied Mathematics and Mechanics. Elsevier, North Holland.
Lemaitre, J., Desmorat, R., 2005. Engineering Damage Mechanics: Ductile, Creep, Fatigue and Brittle Failures. Springer, Berlin.
Moes, N., Dolbow, J., Belytschko, T., 1999. A finite element method for crack without remeshing. Int. J. Numer. Meth. Eng. 46, 131–150.
Needleman, A., 1987. A continuum model for void nucleation by inclusion debonding. J. Appl. Mech. 54, 525–531.
Needleman, A., 1988. Material rate dependence and mesh sensitivity in localization problems. Comput. Meth. Appl. Mech. Eng. 67, 69–85.
Rabotnov, Y.N., 1963. On the equations of state for creep. In: Progress in Applied Mechanics (Prager Anniversary Volume). MacMillan, New York.
Rice, J.R., Wang, J.S., 1989. Embrittlement of interfaces by solute segregation. Mat. Sci. Eng. A 107, 23–40.
Skrzypek, J., Ganczarski, A., 1999. Modeling of material damage and failure of structures. Springer, Berlin.
Trapper, P., Volokh, K.Y., 2008. Cracks in rubber. Int. J. Solids Struct. 45, 6034–6044.
Trapper, P., Volokh, K.Y., 2009. On fracture initiation toughness and crack sharpness for Mode II cracks. Eng. Fract. Mech. 76, 1255–1267.
Trapper, P., Volokh, K.Y., 2010. Modeling dynamic failure in rubber. Int. J. Fracture 162, 245–253.
Tvergaard, V., Hutchinson, J.W., 1992. The relation between crack growth resistance and fracture process parameters in elastic–plastic solids. J. Mech. Phys. Solids 40, 1377–1397.
Volokh, K.Y., 2004. Nonlinear elasticity for modeling fracture of isotropic brittle solids. J. Appl. Mech. 71, 141–143.
Volokh, K.Y., 2007. Hyperelasticity with softening for modeling materials failure. J. Mech. Phys. Solids 55, 2237–2264.
Volokh, K.Y., 2008a. Prediction of arterial failure based on a microstructural bi-layer fiber-matrix model with softening. J. Biomech. 41, 447–453.
Volokh, K.Y., 2008b. Multiscale modeling of material failure: from atomic bonds to elasticity with energy limiters. J. Multiscale Comput. Eng. 6, 393–410.
Volokh, K.Y., Trapper, P., 2008. Fracture toughness from the standpoint of softening hyperelasticity. J. Mech. Phys. Solids 56, 2459–2472.
Volokh, K.Y., Vorp, D.A., 2008. A model of growth and rupture of abdominal aortic aneurysm. J. Biomech. 41, 1015–1021.
Xu, X.P., Needleman, A., 1994. Numerical simulations of fast crack growth in brittle solids. J. Mech. Phys. Solids 42, 1397–1434.
Zhang, P., Klein, P., Huang, Y., Gao, H., Wu, P.D., 2002. Numerical simulation of cohesive fracture by the virtual-internal-bond method. Comput. Model. Eng. Sci. 3, 263–277.